coatings

MDPI

Article

Preparation and Performance of Thermal Insulation Waterborne Polyurethane Coatings Containing 3-Aminopropyltriethoxysilane Modified Organo-Bridged Silica Aerogel

Juan Zhao *, Bohao Yang, Zongren Chen and Yufan Zeng

School of Environmental and Chemical Engineering, Wuyi University, Jiangmen 529020, China; yangbhwyuchem12345@126.com (B.Y.); wyuchemzrchen@163.com (Z.C.); wyuchemzengyf@126.com (Y.Z.)
* Correspondence: wyuchemzj@126.com

Abstract

As an emerging thermal insulation material, silica aerogel holds broad application prospects in building energy conservation. Silica aerogel based waterborne coatings are low thermal conductivity, readily applicable and environmentally friendly, offering significant advantages for improving building energy efficiency. However, the inadequate dispersibility and agglomeration tendency of silica aerogel in aqueous polymer systems adversely affect coating properties. To address this challenge, a waterborne polyurethane (WPU) coating incorporating 3-aminopropyltriethoxysilane-modified organo-bridged silica aerogel (APTES-OBSA) was developed. Integration of organic segments within organo-bridged silica aerogel (OBSA) framework enhanced compatibility of silica aerogel with organic polyurethane chains, thereby reducing aerogel agglomeration. 3-aminopropyltriethoxysilane (APTES) surface modification of OBSA introduced amino groups that strengthened interfacial interaction between OBSA-WPU, effectively enhancing aerogel dispersion within the aqueous polyurethane matrix. APTES-OBSA loading achieved 20 wt% in WPU composite coatings. Compared to neat WPU coating, the composite coatings achieved 21.6% reduction in thermal conductivity, 10 °C lower temperature under thermal irradiation, and 26.6% higher adhesion. Additionally, the composite coatings demonstrated enhanced thermal stability and good water resistance. The excellent comprehensive performance positions this material as a promising eco-friendly thermal insulation coating for building energy-saving applications.

Keywords: organo-bridged silica aerogel; polyurethane; waterborne coating; dispersibility; thermal insulation

check for updates

Academic Editor: Andriy Voronov

Received: 13 August 2025
Revised: 29 August 2025
Accepted: 1 September 2025
Published: 2 September 2025

Citation: Zhao, J.; Yang, B.; Chen, Z.; Zeng, Y. Preparation and Performance of Thermal Insulation Waterborne Polyurethane Coatings Containing 3-Aminopropyltriethoxysilane Modified Organo-Bridged Silica Aerogel. *Coatings* **2025**, *15*, 1021. https://doi.org/10.3390/coatings15091021

Copyright: © 2025 by the authors. Licensee MDPI, Basel, Switzerland. This article is an open access article distributed under the terms and conditions of the Creative Commons Attribution (CC BY) license (https://creativecommons.org/licenses/by/4.0/).

1. Introduction

In the context of global climate change and increasing resource scarcity, energy conservation and environmental protection have become an inevitable trend for the development of building industry [1]. Thermal insulation coatings offer a means to significantly reduce building energy consumption, thus playing an important role in building energy conservation [2,3]. Common thermal insulation coatings used in building include traditional silicate coatings and organic polymer coatings [4,5]. While these coatings can reduce heat conduction to some extent, they possess inherent limitations. For example, silicate coatings exhibit shortcomings such as high brittleness, propensity to cracking, and poor

water resistance, while many organic polymer coatings contain organic solvents that cause environmental pollution [6]. In recent years, with increasing environmental awareness, demand for waterborne coatings in building industry has grown rapidly [7]. By combining the advantages of waterborne coatings and thermal insulation materials, researchers have developed eco-friendly waterborne polymer thermal insulation coatings by incorporating thermal insulation materials as fillers into waterborne polymer matrices [8–10].

Silica aerogel has emerged as a novel insulation material, attracting extensive attention owing to its remarkably low thermal conductivity (as low as 0.012 W/(m·K)) and ultralow density (ranging from 0.003 to 0.4 g/cm^3) [11,12]. The introduction of silica aerogel as insulating fillers into waterborne polymer coatings can effectively enhance their thermal insulation performance [13–15]. However, significant property mismatches between silica region and polymer chain segment pose a challenge for achieving good dispersion of silica aerogel within the aqueous polymeric emulsion. This compromised dispersion degrades the performance of the resultant coatings and limits the development of silica aerogel based waterborne polymer coatings [16,17].

To address this dispersion challenge, surface chemical modification of silica aerogels is the most common strategy [18,19]. Silane coupling agents represent the most frequently employed class of modifiers. Silane coupling agents chemically graft onto silica aerogel surface via a reaction between functional groups of silane coupling agents and hydroxyl groups on aerogel surface [20,21]. This surface chemical modification enhances interfacial interaction between silica aerogel and polymer matrix, consequently promoting improved dispersion of silica aerogel within the polymer matrix [22]. Kim et al. modified the surface of silica aerogel with 3-aminopropyltriethoxysilane (APTES), followed by modification with polymethylene diphenyl diisocyanate (PMDI) to increase the interaction between a polyurethane polymer matrix and the silica aerogel filler. This modification improved the cellular structure of polyurethane foam, resulting in composite foams exhibiting enhanced mechanical and thermal insulation properties. At silica aerogel loading levels $\leq$ 5 wt%, the resulting composite foam exhibited a more uniform and reduced pore size distribution. In comparison with pure polyurethane foam (0 wt% silica aerogel), the modified composite foam demonstrated an increase in maximum compressive strength from 0.125 MPa to approximately 0.23 MPa, while its thermal conductivity decreased from 0.205 W/(m·K) to 0.15 W/(m·K) [23]. Marof et al. modified silica aerogel with silane coupling agent 3-(trimethoxysilyl) propyl methacrylate (KH-570). Incorporating this modified aerogel into cement-based mortar reduced thermal conductivity by up to 55% compared to standard mortar samples [24]. Liu et al. added silane-modified silica aerogel to a waterborne polyurethane acrylate emulsion, optimizing water repellency, heat resistance, and chemical resistance of the derived coating [25]. Despite progress in surface chemical modification, further optimization of silica aerogel modification and application remains necessary.

A review of literature suggests that introducing organic segments into molecular structure of silica can reduce its aggregation tendency and enhance interaction between silica inorganic network and organic polymer chains [26]. Chen et al. introduced polyisobutylene-alt-maleic anhydride and 3-aminopropyltriethoxysilane into the synthesis process of silicone-polyurea elastomers. The resulting compound, containing carbon and silicon chains, strengthened interaction between polyurea segments and siloxane segments, mitigated microphase separation within the silicone-polyurea system, and improved mechanical properties of the polymer [27]. Liu et al. incorporated olefin groups into molecular structure of silica aerogels to achieve a uniform distribution of silica network within a poly(methylmethacrylate) (PMMA) matrix. The enhanced organic-inorganic phase interaction led to improvements in mechanical and thermal performance of PMMA composites [28]. Organo-bridged silica aerogels (OBSA) are members of hybrid silica

aerogel family, in which flexible organic chain was incorporated into molecular skeleton of silica aerogel, endowing aerogel with unique properties such as low density, low thermal conductivity, good hydrophobicity, and flexibility [29,30]. However, there have been few investigations into the effect of OBSA on the dispersibility within waterborne polymer coatings. These motivate our studies on waterborne polymer coatings incorporating OBSA fillers.

In this study, a novel thermal insulation composite coating system was developed based on a waterborne polyurethane (WPU) matrix reinforced with functionalized OBSA fillers. Firstly, OBSA fillers were synthesized via a sol–gel reaction, yielding a molecular framework comprising silica inorganic networks covalently bonded with imide-functionalized mercaptopropyl organic segments. This deliberate organic integration was designed to enhance interfacial interactions between OBSA and polyurethane molecular chains within the coating matrix. Subsequently, the surface of OBSA was further functionalized with APTES to obtain 3-aminopropyltriethoxysilane modified organo-bridged silica aerogel (APTES-OBSA), and amine functionalities on the surface of APTES-OBSA promoted interfacial interactions between polyurethane chains and OBSA particles via hydrogen bonding, markedly improving the dispersibility of OBSA within the coating matrix. The resulting WPU composite coating demonstrated significant thermal insulation properties, along with good adhesion, thermal stability, and water resistance. This combination of properties qualifies it as an eco-efficient thermal barrier coating for building energy conservation applications.

2. Materials and Methods

2.1. Materials

N,N′-(4,4-diphenylmethylene)bismaleimide (BMI, ≥99%), (3-mercaptopropyl)triethoxysilane (MPTES, ≥98%), and 3-aminopropyltriethoxysilane (APTES, ≥98%) were purchased from Shanghai Maikelin Chemical Reagent Co., Ltd., Shanghai, China. Waterborne polyurethane emulsion (WPU F0410, solid content (32 ± 5)%) was obtained from Shenzhen Jitian Chemical Co., Ltd., Shenzhen, China. Hydrochloric acid (37 wt%), acetic acid (99.5%), tetrahydrofuran (THF), triethylamine (TEA), ethanol (EtOH) and n-heptane were supplied by Jiangmen Guoqiao Tech Co., Ltd., Jiangmen, China. Deionized water was prepared in the laboratory. All chemicals were of analytical reagent (AR) grade and used without further purification.

2.2. Preparation of WPU Coatings

2.2.1. Synthesis and Preparation of OBSA

OBSA was synthesized via a sol–gel process based on literature procedures [31]. BMI (14.4 g, 0.04 mol), MPTES (19.2 g, 0.08 mol) and TEA (20 mL) were dissolved in THF (250 mL). The mixture was stirred at room temperature for 12 h, followed by solvent removal. The resulting product was dissolved in a mixture of ethanol (200 mL) and THF (200 mL). deionized water (10 mL) and hydrochloric acid (10 mL) were then added under stirring. The sol was poured into molds and held until gelation occurred. The gel was dried at 60 °C for 72 h, subsequently soaked in EtOH for 48 h followed by n-heptane for 48 h, and finally dried under vacuum to obtain bulk OBSA. The bulk OBSA was ground and sieved (200 mesh) to obtain OBSA powder with particle sizes ranging from 45 μm to 70 μm.

2.2.2. Preparation of APTES-OBSA

OBSA powder (1 g) was dispersed by ultrasonication in a solution containing deionized water (188 g), ethanol (10 g), and APTES (2 g). Acetic acid (1 mL) was added, and

the mixture was stirred at 60 °C for 24 h. APTES-OBSA was obtained after filtration and drying.

2.2.3. Preparation of WPU Composite Coatings

OBSA or APTES-OBSA fillers were dispersed in WPU emulsion at specified mass ratios using moderate magnetic stirring and ultrasonication. The coating formulations are detailed in Table 1.

Table 1. Formulation of WPU composite coatings.

Sample ID	WPU (Mass Ratio, %)	OBSA (Mass Ratio, %)	APTES-OBSA (Mass Ratio, %)
WPU	100	0	0
WPU-OBSA-5	95	5	0
WPU-APTES-OBSA-5	95	0	5
WPU-APTES-OBSA-10	90	0	10
WPU-APTES-OBSA-15	85	0	15
WPU-APTES-OBSA-20	80	0	20

WPU composite coating was poured onto the substrate and subsequently spread using a wet film applicator (SZQ-4, selectable gap widths: 100/200/300/400 μm). A coating thickness of 0.3 mm was precisely controlled by selecting the applicator gap width of 300 μm. Afterwards WPU composite coatings with a thickness of 0.3 mm were applied onto substrates. The preparation process is shown in Figure 1.

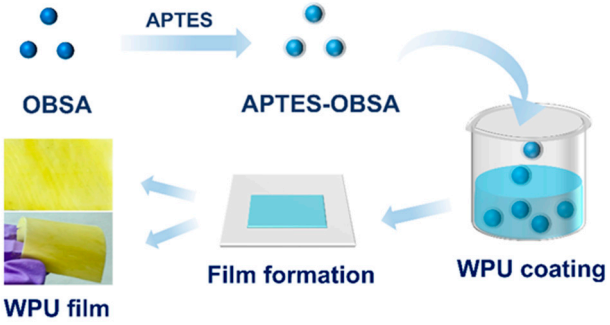


Figure 1. The fabrication scheme of WPU composite coatings containing APTES-OBSA.

2.3. Characterization

Chemical structures were characterized using a Bruker Vertex 70 Fourier transform infrared (FTIR) spectrophotometer at room temperature with 32 scans and resolution of 4 cm^{-1}. Thermogravimetric analysis (TGA) was performed using a NETSZCH TG209F3 thermogravimetric analyzer under N_2 from ambient temperature to 800 °C at a heating rate of 10 °C/min. Contact angles were determined via the sessile drop method on LAUDA Scientific LSA100S-T. The droplets were all 5 μL in volume. Morphology was observed using a TESCAN MIRA LMS high-resolution scanning electron microscope at an accelerating voltage of 2 kV.

2.3.1. Thermal Insulation Test [32]

Thermal insulation performance was evaluated using a laser thermal conductivity meter (Netzsch LFA 467) with a sample size of 10 × 10 mm. Thermal conductivity (λ) was calculated according to the following equation:

$$\lambda(T) = \alpha(T) \cdot C_p(T) \cdot \varrho\ (T) \quad (1)$$

In the formula, λ is thermal conductivity W/(m·K); α is thermal diffusion coefficient $(mm)^2/s$; C_p is specific heat capacity J/(g·K); ϱ is density g/cm^3.

Thermal conductivity change index (n) was a major parameter to quantitatively describe the change in thermal insulation performance of thermal insulation coating, and the calculation formula was as follows:

$$n = (\lambda_x - \lambda_0)/\lambda_0 \times 100\% \quad (2)$$

In the formula, λ_x is thermal conductivity of WPU composite coating W/(m·K); λ_0 is thermal conductivity of pure WPU coating W/(m·K).

To simulate a complex outdoor thermal field environment, a heating lamp with a bulb wattage of 250 W was used to irradiate a coated glass plate (150 × 150 × 8 mm) with a coating diameter of 120 mm and a thickness of 0.3 mm. The heating lamp positioned 20 cm away from the coating surface (simulate a 70 °C thermal field atmosphere). Back-surface temperature of the coated glass plate was monitored using a thermocouple thermometer.

2.3.2. Adhesion Test

Coatings were applied uniformly onto two stainless steel plates with a size of 20 × 50 mm (coated area was 20 × 20 mm), and bonded the coated area together. After drying, specimens were mounted on an INSTRON 3367 universal testing machine. Tensile force was applied axially at a speed of 10 mm/min until separation occurred. The maximum force (F) was recorded. The adhesion was calculated according to the following equation:

$$\sigma = F/S \quad (3)$$

In the formula, σ is adhesion MPa; F is maximum tension value N; S is bonding area mm^2.

2.3.3. Water Absorption Test

Coating films were cutted to a size of 15 × 15 mm, weighed and recorded the mass as m_0. Immersed in deionized water. After 24 h, 48 h, and 72 h, samples were removed, surface moisture wiped off, and reweighed (m). Water absorption was calculated as follows:

$$\text{Water absorption} = (m - m_0)/m_0 \times 100\% \quad (4)$$

3. Results and Discussion

3.1. Chemical Structure Analysis of APTES-OBSA

OBSA was fabricated via sol–gel reaction according to literature, and its molecular structure (Figure 2a) features an organic-inorganic hybrid architecture [31]. To enhance OBSA dispersion in WPU emulsion, the OBSA surface was modified with APTES. During modification, APTES hydrolyzed under acidic conditions using acetic acid as the catalyst, converting Si-OCH_2CH_3 groups to Si-OH groups. These reactive Si-OH groups condensed with surface OH groups on OBSA, chemically grafting APTES onto OBSA (Figure 2b).

Figure 3a showed FTIR spectroscopy of OBSA and APTES-OBSA. OBSA exhibited characteristic peaks at 3475 cm^{-1} (O-H), 2930 cm^{-1} (C-H), 1715 cm^{-1} (C=O), 1610 cm^{-1} (phenyl) [33], and 1110 cm^{-1} (Si-O-Si). APTES-OBSA showed enhanced intensity at 1610 cm^{-1}, which might be attributed to the presence of N–H group (Figure 3b), evidencing APTES incorporation on the silica surface [23].

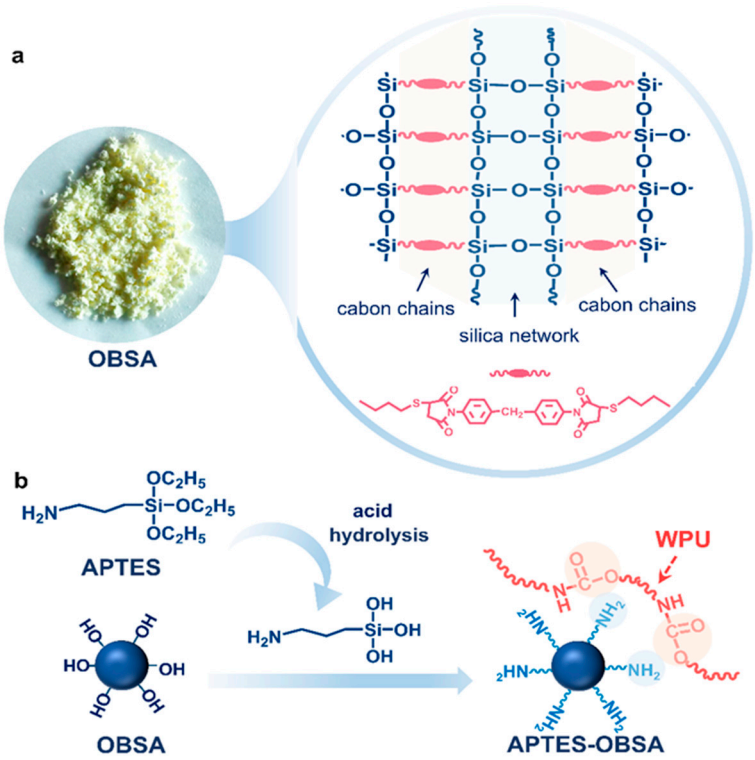


Figure 2. (**a**) Molecular structure of OBSA. (**b**) Schematic illustration of surface chemical modification of OBSA through APTES.

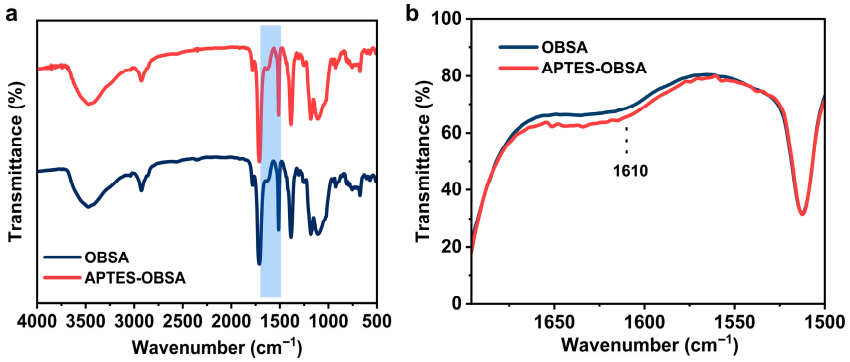


Figure 3. (**a**) FTIR spectra of OBSA and APTES-OBSA. (**b**) Enlarged FTIR spectra of OBSA and APTES-OBSA (wavenumber 1700–1500 cm^{-1}).

The successful surface grafting of APTES onto OBSA was further confirmed by TGA. As shown in Figure 4a, APTES-OBSA exhibited an initial mass loss between 150 and 217 °C, attributable to the volatilization of unreacted APTES [34]. A more pronounced weight loss occurred at 350–600 °C, corresponding to thermal decomposition of both surface-grafted APTES and organosilicon segments within the silica aerogel framework [35]. To quantitatively determine the grafting amount, Figure 4b compared mass loss of OBSA and APTES-OBSA in the 217–600 °C range. By normalizing the weight loss at 217 °C, the surface-grafted APTES content was evaluated to be approximately 7% [34].

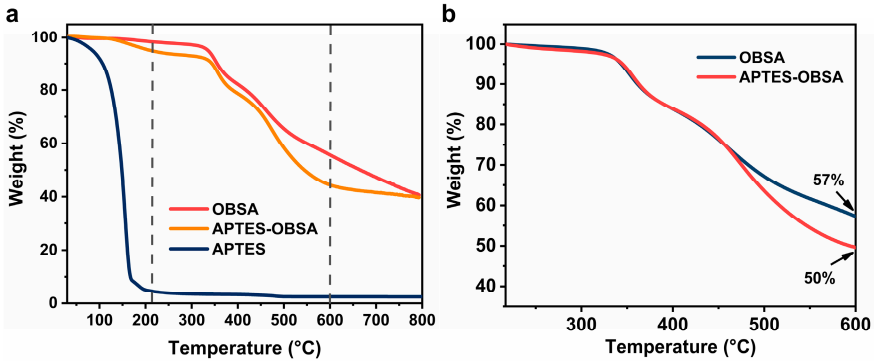


Figure 4. (**a**) TGA curves of APTES, OBSA and APTES-OBSA. (**b**) TGA curves of OBSA and APTES-OBSA normalized by 217 °C (temperature range 217–600 °C).

Good interfacial affinity promotes uniform particle dispersion in liquids [36]. Contact angles (Figure 5) evaluated aerogel-WPU affinity. Both OBSA and APTES-OBSA showed water contact angles of approximately 150°, confirming high hydrophobicity of aerogels. However, WPU emulsion contact angle of OBSA was 75° and WPU emulsion contact angle of APTES-OBSA was 62°, indicating good interface affinity between aerogels and WPU emulsion. This might be attributed to the incorporation of organic chain segments into aerogel molecular structure, which enhanced interactions between organic chains of silica aerogel and polyurethane matrix [26]. The 13° reduction in WPU emulsion contact angle for APTES-OBSA confirmed stronger affinity between APTES-OBSA and WPU emulsion, due to the formation of hydrogen bond between the surface amino groups of APTES and polyurethane chains [37]. These results demonstrated that surface modification of OBSA with APTES improved aerogel-WPU interfacial affinity, which was beneficial for uniform dispersion of APTES-OBSA in WPU coatings.

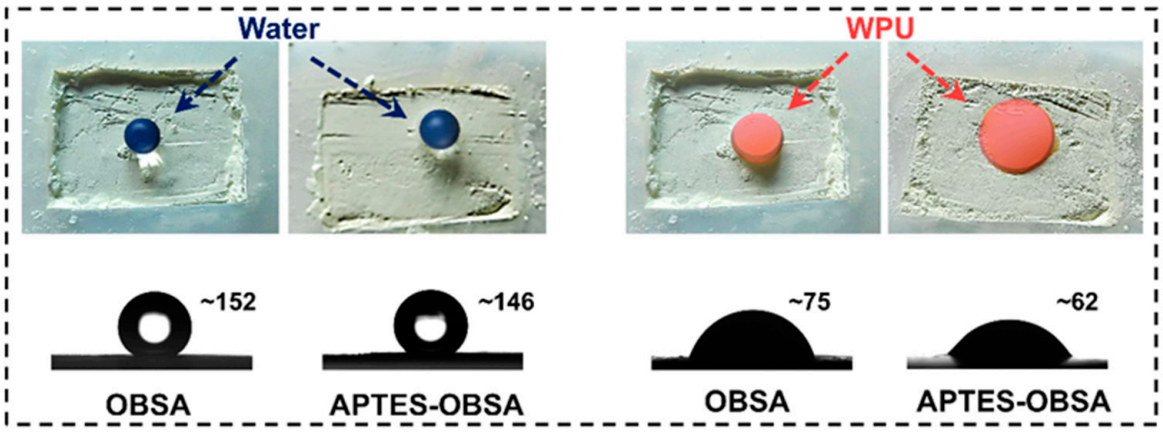


Figure 5. Photographs of water and WPU emulsion droplet formed on the surface of OBSA and APTES-OBSA powder.

3.2. Microstructure of WPU Coatings

During the fabrication process of WPU composite coatings, OBSA and APTES-OBSA were dispersed in WPU matrix through magnetic stirring and ultrasonication. The dispersion states of OBSA and APTES-OBSA within the polymer matrix were characterized by SEM. Figure 6 presented representative SEM micrographs of surface morphologies for the five composite coating formulations.

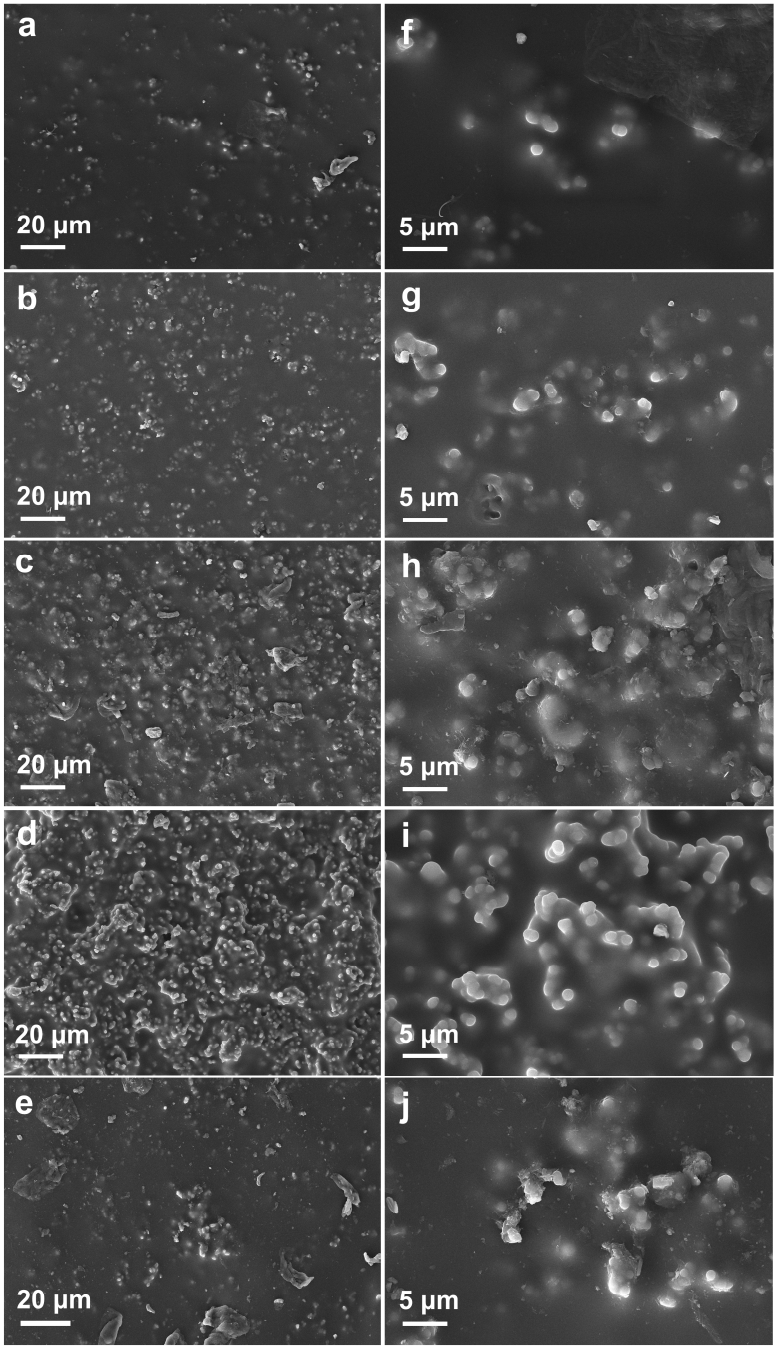


Figure 6. SEM images of WPU composite coatings: (**a**,**f**) WPU-APTES-OBSA-5; (**b**,**g**) WPU-APTES-OBSA-10. (**c**,**h**) WPU-APTES-OBSA-15. (**d**,**i**) WPU-APTES-OBSA-20. (**e**,**j**) WPU-OBSA-5.

At low filler content (WPU-APTES-OBSA-5; 5 wt% filler), the coating surface exhibited smooth morphology with uniformly dispersed fillers (Figure 6a,f). Progressive increase in APTES-OBSA content from 5 wt% to 20 wt% yielded increasing surface roughness (Figure 6a–d,f–i). Although filler density within the matrix increased with loading, the fillers remained uniformly dispersed until reaching 20 wt%, where significant particle accumulation became apparent (Figure 6d,i). The capacity to incorporate up to 20 wt% filler stemed from favorable interfacial affinity between APTES-OBSA and WPU emulsion, ensuring compatibility with the aqueous polyurethane coating matrix [6]. Comparative analysis of WPU-OBSA-5 and WPU-APTES-OBSA-5 revealed distinct morphological differences. Surface micrographs of WPU-OBSA-5 (Figure 6e,j) displayed greater surface

irregularity and localized particle aggregation versus the APTES-modified counterpart, indicating reduced compatibility between unmodified OBSA and WPU matrix.

3.3. Thermal Insulation Performance of WPU Coatings

The thermal conductivity of WPU coatings containing varying APTES-OBSA contents was measured using a laser thermal conductivity analyzer (Figure 7a). Results indicated decreasing thermal conductivity with increasing APTES-OBSA content. Neat WPU coatings exhibited thermal conductivity of 0.227 W/(m·K), while the WPU-APTES-OBSA-5 composite (5 wt% filler) showed a reduced value of 0.187 W/(m·K), representing a 17.62% reduction. This reduction stemmed from the intrinsically low thermal conductivity of APTES-OBSA (0.045 W/(m·K)) and its homogeneous dispersion, which extends heat transfer pathways [17]. Further increases in APTES-OBSA content to 10, 15, and 20 wt% progressively lowered thermal conductivities to 0.182, 0.180, and 0.179 W/(m·K), respectively. However, the rate of reduction diminished at higher loadings. The thermal conductivity decreased by 17.6% at 5 wt% filler relative to neat WPU coating, but only by 21.6% at 20 wt% filler. This diminished efficacy might result from filler aggregation at elevated concentrations, potentially establishing thermal conduction networks that compromise thermal resistance [32]. Comparisons between WPU-OBSA-5 and WPU-APTES-OBSA-5 composites revealed superior performance for the modified filler (Figure 7b). The APTES-modified composite reduced thermal conductivity from 0.227 to 0.187 W/(m·K) (17.62% reduction), compared a reduction to 0.198 W/(m·K) (12.8%) for the unmodified OBSA composite. This confirmed the enhanced thermal insulation efficiency conferred by APTES modification.

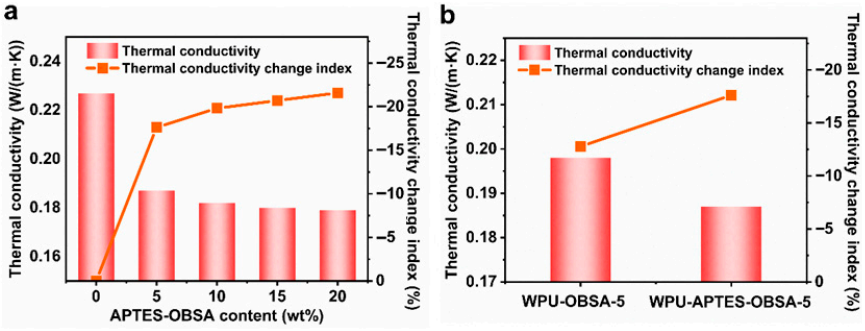


Figure 7. (**a**) Thermal conductivity and thermal conductivity change index of WPU coatings with different filler content of APTES-OBSA. (**b**) Thermal conductivity and thermal conductivity change index of WPU-OBSA-5 and WPU-APTES-OBSA-5.

To quantitatively evaluate thermal insulation performance, simulated outdoor thermal field tests were conducted at 70 °C using a heating lamp (Figure 8a). A 0.3 mm-thick unmodified WPU coating applied to the glass plate exhibited a temperature of 46 °C on the back-surface of the glass plate after 40 min irradiation. In contrast, APTES-OBSA composites (5–20 wt%) stabilized at temperatures between 36 and 37 °C within the same period-approximately 10 °C lower than neat WPU coating. This significant differential demonstrated exceptional thermal insulation performance. Comparative testing of WPU-OBSA-5 and WPU-APTES-OBSA-5 confirmed superior performance for the modified filler (Figure 8a). After 40 min irradiation, WPU-OBSA-5 reached 39 °C, which was 2 °C higher than its APTES-modified counterpart. This discrepancy was attributed to inhomogeneous dispersion of unmodified OBSA particles, forming localized conductive pathways that degrade insulation [32]. The influence of coating thickness on thermal insulation performance was evaluated. As shown in Figure 8b, coating thickness exhibited no significant effect on back-surface temperature of glass substrate within the initial 15 min of irradiation, whereas a gradual temperature reduction occurred with increasing coating thickness after 40 min.

A liner relationship was observed where each 0.1 mm increase in coating thickness corresponded to a 1 °C decrease in temperature. These findings collectively demonstrated that both OBSA and APTES-OBSA were able to enhance thermal insulation, with APTES-OBSA exhibiting superior efficacy-consistent with thermal conductivity measurements. Among the formulations, the 10 wt% APTES-OBSA composite offered optimal application value from the perspective of balancing cost and performance.

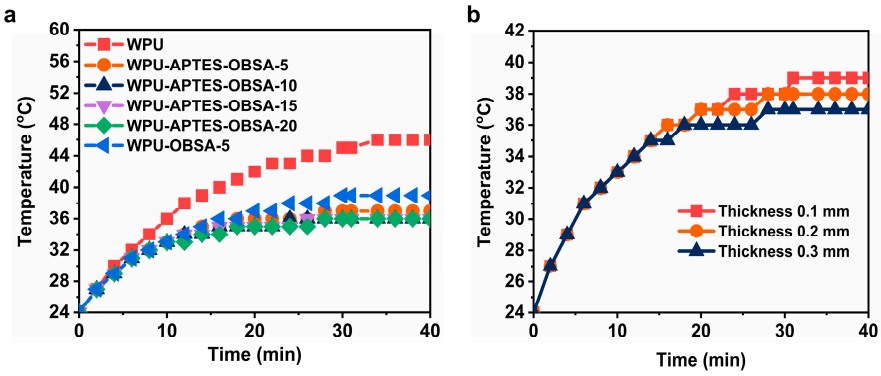


Figure 8. (**a**) Back-surface temperature curves of WPU coatings with different filler content of OBSA and APTES-OBSA. (**b**) Back-surface temperature curves of WPU coatings with different thicknesses.

3.4. Thermal Stability of WPU Coatings

The effect of APTES-OBSA content on the thermal stability of WPU coatings was analyzed by TGA under a nitrogen atmosphere, with the resulting TG and DTG curves presented in Figure 9. In N_2 atmosphere, all the coatings initiated thermal degradation at approximately 360 °C, indicating their high thermal stability. The maximum thermal degradation temperature for neat WPU coating occurred at 393 °C, corresponding to chain scission in the polymer matrix. Neat WPU coating exhibited a residual char yield of 2.4% at 800 °C, demonstrating minimal char formation from matrix degradation. Conversely, APTES-OBSA-filled WPU coatings showed significantly increased residual char yields at 800 °C (Figure 9a), which increased progressively with the increase in filler loading. At 20 wt% APTES-OBSA, the char yield reached 13.4%, attributable to char formation during thermal decomposition of the fillers APTES-OBSA (Figure 4a) [38]. Furthermore, APTES-OBSA addition increased the maximum thermal degradation temperature by 4–5 °C (Figure 9b). For instance, WPU-APTES-OBSA-20 exhibited a maximum degradation temperature of 398 °C, which was 5 °C higher than neat WPU coating. This enhancement resulted from combined effect of the inherent thermal stability of aerogel fillers and the filler's impedance to pyrolysis of WPU polymer chains [21]. These results demonstrated improved thermal stability through APTES-OBSA incorporation.

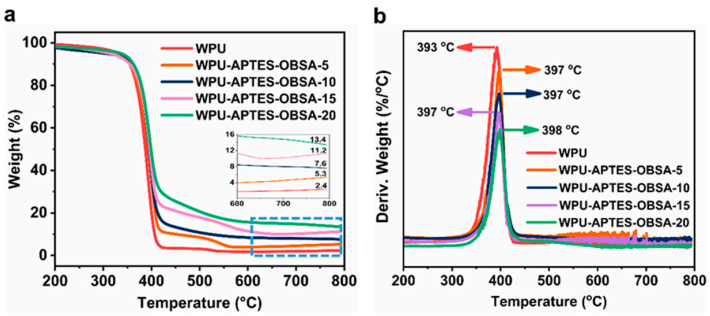


Figure 9. (**a**) TGA curves of WPU coatings with different filler content of APTES-OBSA under N_2 atmosphere. (**b**) DTG curves of WPU coatings with different filler content of APTES-OBSA under N_2 atmosphere.

3.5. Adhesion of WPU Coatings

Adhesion performance represented a crucial practical criterion for evaluating coating usability. Good adhesion ensured tight bonding between coating and substrate. The adhesion strength was measured using a universal testing machine. As shown in Figure 10a, neat WPU coating (0 wt% APTES-OBSA) exhibited an adhesion strength of 5.158 MPa. At 5 wt% and 10 wt% filler loading, the adhesion increased to 5.731 MPa and 6.528 MPa, respectively, owing to enhanced interfacial bonding between APTES-OBSA and the WPU coating matrix [6]. However, further increasing APTES-OBSA to 15–20 wt% reduced adhesion to 5.746–5.661 MPa, as excessive filler loading exceeded the matrix's binding capacity [35]. Overall, composite coatings incorporating APTES-OBSA exhibited higher adhesion strength relative to neat WPU coatings.

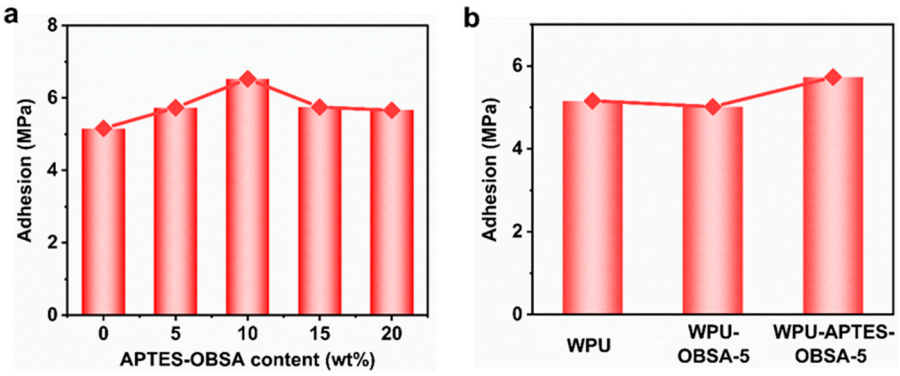


Figure 10. (**a**) adhesion of WPU coatings with different filler content of APTES-OBSA. (**b**) adhesion of coatings WPU, WPU-OBSA-5 and WPU-APTES-OBSA-5.

To assess OBSA modification effects, Figure 10b compared the adhesion strength of WPU-OBSA-5 (5.017 MPa) and WPU-APTES-OBSA-5 (5.731 MPa). Compared to neat WPU coating, these represented a 2.7% decrease and 11.1% increase, respectively, indicating relatively poor inferior interfacial compatibility of OBSA. Thus, APTES-OBSA enhanced coating adhesion compared to unmodified OBSA. Notably, at 10 wt% APTES-OBSA, coating adhesion increased by up to 26.6% relative to neat WPU coating.

3.6. Water Resistance of WPU Coatings

Water resistance critically impacted coating application prospects, and we evaluated water resistance of WPU films after 24 h, 48 h, and 72 h immersion. All the specimens remained free of blistering, cracking, and mildew after 72 h immersion, demonstrating inherent water resistance. Water absorption rate serves as a key indicator for evaluating coating water resistance. As shown in Figure 11a, the effect of varying APTES-OBSA content on water absorption rate exhibited a distinct trend, and water absorption rates initially increased with higher filler loading before gradually decreasing. At 10 wt% APTES-OBSA content, maximum water absorption rate reached 9.52% after 72 h immersion, attributed to enhanced interfacial affinity that increased water uptake at lower loadings. Beyond this threshold, densely packed silica aerogel particles inhibited internal diffusion of water, progressively reducing water absorption [35].

Comparative analysis in Figure 11b showed the WPU-OBSA-5 coating (5 wt% OBSA) achieved water absorption rates of 5.05% (24 h immersion) and 7.19% (72 h immersion), while neat WPU coating registered 5.5% and 7.18% at identical immersion times, exhibiting almost the same water absorption rate after 72 h immersion. However, the significantly lower 24 h water absorption rate of WPU-OBSA-5 indicated its slower initial water uptake. This delayed water absorption suggested hindered internal water diffusion in the coating, likely attributable to compromised filler-matrix interfaces within the composite coating.

Conversely, WPU-APTES-OBSA-5 showed significantly elevated water absorption rate of 6.58% (24 h immersion) and 9.04% (72 h immersion), representing 19.6% and 25.9% increases over neat WPU coating, respectively. This increase resulted from APTES modification enhancing interfacial affinity, which facilitated water penetration throughout the composite coating and thereby increased overall water absorption.

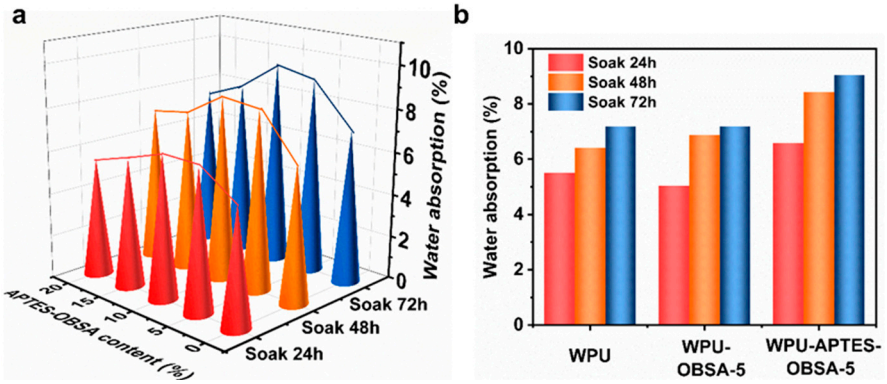


Figure 11. (**a**) Water absorption of WPU coatings with different filler content of APTES-OBSA. (**b**) Water absorption of coatings WPU, WPU-OBSA-5 and WPU-APTES-OBSA-5.

4. Conclusions

In this work, a functional thermal insulation coating was successfully prepared using WPU emulsion as film-forming matrix and APTES-OBSA particles as fillers.

(1) APTES-OBSA was obtained through surface functionalization of OBSA using silane coupling agent APTES as modifying agent. FTIR and TGA confirmed the successful grafting of APTES onto OBSA surfaces. Contact angle measurements demonstrated good interfacial compatibility between APTES-OBSA and WPU emulsion. SEM investigation of WPU coatings incorporating APTES-OBSA revealed superior dispersion of the modified particles in the aqueous polyurethane matrix.

(2) Performance evaluation indicated that both OBSA and APTES-OBSA could reduce thermal conductivity and enhance thermal insulation performance of WPU coatings, with APTES-OBSA exhibiting superior performance enhancement. Compare to neat WPU coatings, APTES-OBSA/WPU composite coating achieved up to 21.6% reduction in thermal conductivity. Glass substrate coated with 0.3 mm -thick APTES-OBSA/WPU coating exhibited 10 °C lower back-surface temperatures than neat WPU coating after 40 min irradiation at 70 °C.

(3) APTES-OBSA also endowed WPU coatings with higher thermal stability, manifested by an 11% increase in char residue at 800 °C and a 5 °C increase in maximum thermal decomposition temperature. Moreover, APTES-OBSA increased coating adhesion by up to 26.6%, whereas OBSA resulted in a slight decrease in adhesion. All silica aerogel/WPU composites exhibited satisfactory water resistance, and the incorporation of APTES-OBSA (5–20 wt%) resulted in a marginal increase (0.39–2.34%) in water absorption rate after 72 h immersion.

In short, the fabricated APTES-OBSA/WPU composite coatings demonstrated a well-balanced performance profile, serving it as an eco-friendly thermal insulation material for building thermal management. Considering both cost efficiency and performance factors, WPU-APTES-OBSA-10 demonstrates optimal potential for practical applications.

Author Contributions: Methodology, B.Y. and Z.C.; investigation, Y.Z.; writing—original draft preparation, B.Y.; writing—review and editing, J.Z.; supervision, J.Z.; project administration, B.Y.; funding acquisition, J.Z. All authors have read and agreed to the published version of the manuscript.

Funding: This research was funded by Guangdong Leicengkeji Co., Ltd. funded project (HX22140) and College Students' Innovative Entrepreneurial Training Plan Program of Wuyi University (X202511349090).

Institutional Review Board Statement: Not applicable.

Informed Consent Statement: Not applicable.

Data Availability Statement: The authors confirm that the data supporting the findings of this study are available within the article.

Conflicts of Interest: The authors declare no conflicts of interest.

References

1. Peng, Y.; Fan, L.; Jin, W.; Ye, Y.; Huang, Z.; Zhai, S.; Luo, X.; Ma, Y.; Tang, J.; Zhou, J. Coloured low-emissivity films for building envelopes for year-round energy savings. *Nat. Sustain.* **2022**, *5*, 339–347. [CrossRef]
2. Ye, X.; Chen, D. Thermal insulation coatings in energy saving. In *Energy-Efficient Approaches in Industrial Applications*, 1st ed.; IntechOpen: London, UK, 2019; Volume 1, pp. 8–15. [CrossRef]
3. Simpson, A.; Fitton, R.; Rattigan, I.G.; Marshall, A.; Parr, G.; Swan, W. Thermal performance of thermal paint and surface coatings in buildings in heating dominated climates. *Energ. Build.* **2019**, *197*, 196–213. [CrossRef]
4. Saienko, N.; Bikov, R.; Skripinets, A.; Demidov, D.; Dukarov, S. Effectiveness evaluation of silicate fillers for the creation of thin-layer thermal insulation coatings. *AIP Conf. Proc.* **2023**, *2490*, 050021. [CrossRef]
5. Ma, Z.; Liu, X.; Xu, X.; Liu, L.; Yu, B.; Maluk, C.; Huang, G.; Wang, H.; Song, P. Bioinspired, highly adhesive, nanostructured polymeric coatings for superhydrophobic fire-extinguishing thermal insulation foam. *ACS Nano* **2021**, *15*, 11667–11680. [CrossRef]
6. Zhang, Z.; Han, X.; Jia, L.; Yu, W.; Zheng, Q. Highly water-resistant transparent waterborne polyurethane thermal-insulation coating material with multiple self-crosslinking network based on controllably activated end-capping reagent. *Prog. Org. Coat.* **2024**, *187*, 108104. [CrossRef]
7. Dong, W.; Ma, M. Recent developments and advanced applications of promising functional nanocomposites for green buildings: A review. *J. Build. Eng.* **2025**, *102*, 111905. [CrossRef]
8. Yan, X.; Wang, L.; Qian, X. Influence of the PVC of glass fiber powder on the properties of a thermochromic waterborne coating for Chinese fir boards. *Coatings* **2020**, *10*, 588. [CrossRef]
9. Chen, C.; Yu, D.; Yuan, Q.; Wu, M. Anisotropic, elastic cellulose nanofibril cryogel cross-linked by waterborne polyurethane with excellent thermal insulation performance. *Cellulose* **2022**, *29*, 6219–6229. [CrossRef]
10. Calovi, M.; Rossi, S. Durability and thermal behavior of functional paints formulated with recycled-glass hollow microspheres of different size. *Materials* **2023**, *16*, 2678. [CrossRef]
11. Xiang, Y.; Yan, M.; Li, L.; Xiao, Y.; Sun, H.; Zhang, Z.; Yang, H.; Cheng, X.; Pan, Y. Low thermal conductivity and self-cleaning silica aerogel coating based on a secondary coating encapsulation strategy. *Constr. Build. Mater.* **2025**, *472*, 140878. [CrossRef]
12. Wang, Y.; Dai, X.; Kong, Y.; Shen, X. Fatigue resistant flexible silica aerogel for thermal sealing under force-heat coupling conditions. *J. Non-Cryst Solids* **2025**, *665*, 123618. [CrossRef]
13. Li, Z.; Chen, Z.; Duan, Y.; Chen, J.; Yao, S.; Peng, L.; Chen, W.; Menshutina, N.; Liu, M. A review of silica aerogel based thermal insulation coatings: Preparation, properties and applications. *Prog. Org. Coat* **2025**, *208*, 109449. [CrossRef]
14. de Sousa, F.V.; Fortunato, D.D.S.; Grosso, M.; Barcia, O.E.; Quintela, J.P.; Margarit-Mattos, I.C. Thermal insulation paintings: Viscoelastic and corrosion-related properties. *Prog. Org. Coat* **2025**, *200*, 109084. [CrossRef]
15. Ran, Q. Foamy melamine resin-silica aerogel composite-derived thermal insulation coating. *Nanomaterials* **2025**, *15*, 135. [CrossRef]
16. Riahipour, R.; Nemati, M.S.; Zadehmohamad, M.; Baniassadi, M. Mechanical properties of an epoxy-based coating reinforced with silica aerogel and ammonium polyphosphate additives. *Polym. Polym. Compos.* **2022**, *30*, 1–10. [CrossRef]
17. Goryunova, K.I.; Gahramanli, Y.N. Insulating materials based on silica aerogel composites: Synthesis, properties and application. *RSC Adv.* **2024**, *14*, 34690–34707. [CrossRef]
18. Kim, Y.J. Ambient drying silica aerogel coatings modified with polyethylene glycol. *J. Ceram. Process. Res.* **2017**, *18*, 55–58.
19. Halim, Z.A.A.; Yajid, M.A.M. Comparison of dynamic mechanical properties and thermal conductivity of unsaturated polyester composites filled with plain SiO_2 aerogel and core-shell SiO_2 aerogel. *Mater. Today Proc.* **2019**, *17*, 686–693. [CrossRef]
20. Wang, W.; Yu, X.; Lai, C.; Li, G.; Zhu, P.; Sun, R. Systematic study of the effect of silane coupling agent on the hydrothermal aging resistance of the underfill epoxy resin and silica interface via molecular dynamics simulation. *Appl. Surf. Sci.* **2025**, *688*, 162313. [CrossRef]
21. Li, X.; Chen, J.; Yang, L.K. Silane modification of nanofibrillated cellulose and its effect on the properties of waterborne acrylic resin. *J. Appl. Polym. Sci.* **2023**, *140*, e54543. [CrossRef]
22. Zou, H.; Wu, S.; Shen, J. Polymer/silica nanocomposites: Preparation, characterization, properties, and applications. *Chem. Rev.* **2008**, *108*, 3893–3957. [CrossRef]

23. Lee, D.I.; Ha, Y.; Jeon, H.; Kim, S.H. Preparation and properties of polyurethane composite foams with silica-based fillers. *Appl. Sci.* **2022**, *12*, 7418. [CrossRef]
24. Marof, K.; Iller, L. Enhancing thermal insulation in cement mortar with silica aerogel and recycled PET plastic. *Constr. Build. Mater.* **2025**, *467*, 140320. [CrossRef]
25. Xu, L.; Liu, Y.; Xin, B.; Zhou, Y. Preparation and properties of functional fabric coating based on SiO_2-aerogel/polyurethane. *Fiber. Polym.* **2022**, *23*, 1870–1880. [CrossRef]
26. Al-Kandary, S.; Ali, A.A.M.; Ahmad, Z. Morphology and thermo-mechanical properties of compatibilized polyimide-silica nanocomposites. *J. Appl. Polym. Sci.* **2005**, *98*, 2521–2531. [CrossRef]
27. Chen, Y.; Yang, K.; Dong, H.; Niu, H.; Wang, Q.; Cheng, Q. Synthesis and characterization of silicone polyurea and mechanical properties improvement through interfacial reaction. *RSC Adv.* **2025**, *15*, 11835–11844. [CrossRef]
28. Li, H.; Li, R.; Liu, H.; Li, J.; Yang, A. Heat transport across phase interface in silica aerogel/polymethyl methacrylate composites. *Polym. Test.* **2019**, *76*, 326–332. [CrossRef]
29. Meti, P.; Wang, Q.; Mahadik, D.B.; Lee, K.Y.; Gong, Y.D.; Park, H.H. Evolutionary progress of silica aerogels and their classification based on composition: An overview. *Nanomaterials* **2023**, *13*, 1498. [CrossRef] [PubMed]
30. Abebe, A.M.; Biesuz, M.; Vakifahmetoglu, C.; Cassetta, M.; Sorarù, G.D. Hybrid silica aerogels from bridged silicon alkoxides: Ultralow thermal conductivity for low-temperature applications. *J. Sol-Gel Sci. Tech.* **2025**, *114*, 1117–1126. [CrossRef]
31. Zhao, J.; Zeng, G.; Zou, F.; Jiang, S.; Chen, Y.; Wang, H.; Mu, C.; Tang, X.-Z. Bismaleimide bridged silsesquioxane aerogels with excellent heat resistance: Effect of sol–gel solvent polarity. *Soft Matter* **2020**, *16*, 3548–3554. [CrossRef] [PubMed]
32. Wang, Z.; Gong, G.; Gao, L.; Cui, W.; Wang, Y. Preparation and performance of intumescent water-based coatings with both thermal insulation and flame retardant functions. *Chem. Eng. J.* **2024**, *480*, 148165. [CrossRef]
33. Yang, H.; Ye, L.; Gong, J.; Li, M.; Jiang, Z.; Wen, X.; Chen, H.; Tian, N.; Tang, T. Simultaneously improving the mechanical properties and flame retardancy of polypropylene using functionalized carbon nanotubes by covalently wrapping flame retardants followed by linking polypropylene. *Mater. Chem. Front.* **2017**, *1*, 716–726. [CrossRef]
34. Gonçalves, I.A.; Barauna, J.; Pinheiro, I.F.; Calderaro, M.P.; Morales, A.R. Nanocomposites of poly(butylene adipate-co-terephthalate) containing sepiolite modified with 3-aminopropyltriethoxysilane and octadecyl isocyanate. *J. Appl. Polym. Sci.* **2023**, *140*, e54642. [CrossRef]
35. He, S.; Wu, X.; Zhang, X.; Sun, J.; Tian, F.; Guo, S.; Du, H.; Li, P.; Huang, Y. Preparation and properties of thermal insulation coating based on silica aerogel. *Energ. Build.* **2023**, *298*, 113556. [CrossRef]
36. Hudak, N.S.; Manas-Zloczower, I.; Feke, D.L. Methodology and analysis of the effect of liquid infiltration on the hydrodynamic dispersion of silica aerogel agglomerates. *Kona* **2004**, *22*, 134–142. [CrossRef]
37. Di, Z.; Ma, S.; Wang, H.; Guan, Z.; Lian, B.; Qiu, Y.; Jiang, Y. Modulation of thermal insulation and mechanical property of silica aerogel thermal insulation coatings. *Coatings* **2022**, *12*, 1421. [CrossRef]
38. Gu, J.; Fu, R.; Kang, S.; Yang, X.; Song, Q.; Miao, C.; Ma, M.; Wang, Y.; Sai, H. Robust composite aerogel beads with pomegranate-like structure for water-based thermal insulation coating. *Constr. Build. Mater.* **2022**, *341*, 127722. [CrossRef]

Disclaimer/Publisher's Note: The statements, opinions and data contained in all publications are solely those of the individual author(s) and contributor(s) and not of MDPI and/or the editor(s). MDPI and/or the editor(s) disclaim responsibility for any injury to people or property resulting from any ideas, methods, instructions or products referred to in the content.